nature communications

Article

https://doi.org/10.1038/s41467-025-58338-9

Advanced enzyme-assembled hydrogels for the remediation of contaminated water

Received: 27 January 2025

Accepted: 19 March 2025

Published online: 28 March 2025

Check for updates

Jinlong Zhang[1], Jason C. White[2], Gregory V. Lowry[3], Jinglei He[1], Xuefeng Yu[1], Chuanhao Yan[1], Liang Dong[1], Shu Tao[1] & Xilong Wang[1]

Enzyme-catalyzed biodegradation is an emerging green strategy for environmental remediation, although challenged by high cost and poor robustness. Herein, natural biopolymer (cellulose)-derived hydrogels concurrently doped with β-cyclodextrin and montmorillonite nanosheets that are synthesized in one-step demonstrate exceptional pollutant affinity and mechanical strength. Laccase is then stably and effectively assembled onto the hydrogels by a facile strategy based on charge-assisted H-bonding, which can be extended to other enzymes. The advanced laccase-assembled hydrogels display excellent stability and increased degradation activity achieved by strong substrate capture and rapid electron transfer. The laccase-assembled hydrogels exhibit significantly improved removal (62-fold) and degradation (52-fold) performance compared to free laccase for diverse organic pollutants (e.g., polycyclic aromatic hydrocarbons) in real wastewater. This enhanced performance is maintained despite the presence of heavy metals, other organic chemicals or dissolved organic matter. This work provides a practical strategy for designing an advanced and sustainable biodegradation tool for environmental remediation.

Water pollution poses a significant and increasing threat to human and ecosystem health[1,2], particularly when contaminated by persistent organic pollutants (POPs) with high potential for toxicity, bioaccumulation, and long-distance migration[3]. Biodegradation is often a promising strategy for pollutant removal from water[4,5], owing to its greater environmental friendliness relative to more traditional chemical methods. However, the application of biodegradation is limited by a range of factors, including complex cultivation processes and harsh operating conditions[6]. Since biodegradation is enabled by enzymatically driven processes, the direct use of enzymes to degrade pollutants could overcome a number of operational difficulties[7,8]. However, their sensitive tertiary structure and high-water solubility often leads to rapid denaturation and deactivation under environmental conditions, thereby compromising degradation performance. In addition, recycling at the molecular level is difficult; these factors jointly increase treatment cost[9].

Recent efforts have focused on immobilizing enzymes on various carriers to preserve activity and promote recylclability[10–12]. Among these platforms, hydrogels exhibit great promise as 3-dimensional polymer carriers and importantly, soft/wet materials are conducive to preserving protein function due to their resemblance to a natural extracellular matrix structure[10,13]. However, the relatively poor mechanical strength limits their recycling potential[14] and could increase the risk of secondary pollution[15]. In addition, hydrogels with hydrophilic properties will have relatively low affinity for POPs, thereby limiting their efficacy to facilitate subsequent degradation by enzymes. Moreover, technical difficulties related to the synthesis of hydrogel-like carrying materials for enzyme immobilization, including high cost and lack of environmental sustainability, need to be addressed[16]. So, ensuring the carrying material has high affinity for POPs, high mechanical strength, and overall sustainability remain long-standing challenges to be overcome.

[1]Laboratory for Earth Surface Processes, College of Urban and Environmental Sciences, Peking University, Beijing, China. [2]The Connecticut Agricultural Experiment Station, New Haven, CT, USA. [3]Department of Civil and Environmental Engineering, Carnegie Mellon University, Pittsburgh, PA, USA.
e-mail: xilong@pku.edu.cn

More specifically, the challenges of efficiently and stably immobilizing an enzyme on or in a carrier, ensuring a substantial loading amount, and avoiding significant changes of its 3-dimensional conformation resulting from strong binding to the carrier that would compromise degradation performance must be addressed[17,18]. Recently, several studies have reported on charge-assisted hydrogen bonds (CAHB), which are distinct short strong H-bonding with covalent bond properties (up to 48%)[19–21] that can be formed between a favorably oriented and charged donor-acceptor pair that have similar proton affinity or point of zero charge ($|\Delta pK_a|$ or $|\Delta PZC| < \sim 5.0$, Supplementary Note 1)[22,23]. CAHB is over 5 times stronger than ordinary H-bonding but weaker than covalent bonds; such a level of activity could promote stable immobilization of ionizable organic chemicals on various materials (such as carbon nanomaterials and amine-modified resin)[23–25]. With this intriguing potential, we hypothesize that enzymes can be stably and abundantly assembled on hydrogels with similar pK_a or PZC via CAHB, thereby maintaining optimal degradation performance and achieving high activity, stability, and cost-effectiveness. Additionally, ensuring the enzyme-assembled hydrogels have stable degradation performance under a wide pH and temperature range, the presence of multiple interferences (e.g., dissolved organic matter, heavy metals, or other organic pollutants) even authentic wastewater, as well as storage stability, excellent redox potential and electron transfer rate, are also questions that must be answered before practical application.

Here we synthesized a biopolymer cellulose-based hydrogel concurrently doped with β-cyclodextrin (CD) (Supplementary Fig. 1) to capture POPs (USEPA priority polycyclic aromatic hydrocarbons, PAHs) and montmorillonite nanosheets (MMT) to enhance the mechanical strength (Cellulose-CD-MMT). Importantly, an advanced and extensible enzyme immobilization strategy (CAHB) was employed to effectively assemble laccase onto the hydrogels to achieve degradation of diverse organic pollutants (e.g., PAHs, antibiotics, per- and polyfluoroalkyl substances: PFAS) with excellent performance under various complex exposure scenarios involving authentic wastewater. The advanced composite hydrogels overcome many of the aforementioned challenges, thereby providing an impactful design framework for sustainable contaminant biodegradation in aqueous systems and guiding future development of immobilized-enzyme technologies such as programmable protein designs as next-generation remediation strategies.

Results

Fabrication and characterization of hydrogels

Cellulose-CD hydrogels were synthesized by doping CD onto cellulose with the cross-linker 1,4-butanediol diglycidyl ether (BDE) to capture POPs to facilitate their degradation (e.g., phenanthrene: Phe, Fig. 1a, Supplementary Fig. 2). CD doping significantly increased the partitioning coefficient (K_d, up to 1.52×10^4 L kg^{-1}) and density functional theory (DFT)-calculated sorption energy (E_{sorp}, −87.13 kJ mol^{-1}, host-guest interaction) of Phe by the hydrogels relative to the undoped form (Fig. 1a, Supplementary Fig. 3). This indicates that CD doping provided abundant association sites and captured contaminant molecules partitioning into the hydrophobic cavity, likely enabling subsequent degradation by the immobilized enzyme. The concurrent doping CD and MMT to form Cellulose-CD-MMT hydrogels balanced increased mechanical strength while still maintain strong Phe affinity (Fig. 1b, Supplementary Figs. 4–5). Notably, the Cellulose-CD-MMT hydrogels synthesized with the optimal doped amount of CD and MMT had not only the greatest affinity for Phe (K_d: 1.52×10^4 L kg^{-1}) but also the greatest compressive strength (2.19 MPa), outperforming most materials reported in the literature (Supplementary Table 1). The N_2 sorption-desorption isotherms and pore size distribution of the Cellulose-CD-MMT hydrogels indicate a mesoporous structure that is conducive to the exposure of active sites for pollutant capture and laccase assembly (Supplementary Fig. 6). Field-emission scanning electron microscopy coupled with energy dispersive spectroscopy (FESEM-EDS) images (Fig. 1c–g, Supplementary Fig. 7) of Cellulose-CD-MMT hydrogels show a robust 3D porous network with uniform distribution of C, O, Si, and Al on the surfaces. This suggests homogeneous entanglement between MMT and cellulose or CD, leading to strong interactions and the associated high mechanical strength of the Cellulose-CD-MMT hydrogels.

X-ray diffraction (XRD) analysis indicates that MMT doping disrupted the crystalline structure of cellulose in Cellulose-CD-MMT hydrogels, while that of CD remains unchanged (Fig. 1h), suggesting partial disruption of H-bonding in cellulose. The characteristic peak for MMT shifted from 7.2° to 6.2°, indicating doping increased its interlayer spacing[26]. Fourier transform infrared spectroscopy (FTIR) results show a distinct peak at 837 cm^{-1} on Cellulose-CD-MMT hydrogels after MMT doping (Fig. 1i), indicating C-O-Al bond formation between MMT and cellulose[27]. Two peaks at 74.2 and 75.0 eV on the Al 2p X-ray photoelectron spectroscopy (XPS) spectra of MMT corresponded to AlO_4 (tetrahedrally coordinated aluminum) and AlO_6 (octahedrally coordinated aluminum), respectively[28,29] (Fig. 1j). The AlO_6/AlO_4 signal intensity ratio (r_{si}) on the Al 2p spectra of Cellulose-CD-MMT hydrogels (4.42) was higher than that of MMT (2.47), with increased binding energies (0.3 eV) of AlO_6 and AlO_4. This is because MMT doped on Cellulose-CD-MMT hydrogels coordinated with cellulose through C-O-Al bonds, leading to significant conversion from AlO_4 to AlO_6, further supported by their O 1 s, C 1 s, and Si 2p spectra (Supplementary Fig. 8) and previous work[30]. The aforementioned results collectively demonstrate that the Al produced by isomorphic substitution (Si→Al) on the MMT surface facilitates the formation of C-O-Al bonds with cellulose, leading to the conversion from AlO_4 to AlO_6, disruption of cellulose H-bonds and enhancement of mechanical strength of the resulting Cellulose-CD-MMT hydrogels.

Strength and stability of the interactions between MMT and cellulose were further evaluated by DFT calculations. The coordination intensity between cellulose and MMT (−94.16 kJ mol^{-1}, Fig. 1k) was 4.38 times that of cellulose and itself (−21.50 kJ mol^{-1}). This consistently supports the facile formation of strong C-O-Al bonds (AlO_6) between MMT and cellulose, which consequently disrupts the H-bond network in cellulose. Additionally, the energy gap ($E_{gap} = E_{LUMO} - E_{HOMO}$, a stability indicator) value (4.82 eV) between cellulose and MMT is greater than that between cellulose and itself (3.70 eV) (Supplementary Fig. 9), indicating higher stability of the coordination between cellulose and MMT[31,32]. The above experimental and simulation results consistently demonstrate the exceptional mechanical strength of Cellulose-CD-MMT hydrogels, attributed to the robust and stable coordination between cellulose and MMT (Fig. 1l). Importantly, the Cellulose-CD-MMT hydrogels also show significant potential for enzyme assembly, which is further discussed below.

Laccase assembly and CAHB formation between laccase and Cellulose-CD-MMT hydrogels

Variation in the amount of assembled laccase on the Cellulose-CD-MMT hydrogels and its enzymatic activity as a function of its dose was explored (Fig. 2a, Supplementary Fig. 10). The maximum laccase loading (754.5 mg g^{-1}) on Cellulose-CD-MMT hydrogels exceeds most literature-reported values (Supplementary Table 2). Analyses via ^{1}H nuclear magnetic resonance spectroscopy (^{1}H NMR), confocal laser scanning microscopy (CLSM) and FTIR verified successful laccase assembly (Supplementary Figs. 11–12, Supplementary Table 3). The assembled laccase exhibited a broader operational range (pH 3–7, 15–55 °C) relative to free laccase (pH 3–4, 35–45 °C) with over 80% activity retention (Fig. 2b, c). Optimal pH (5.0) and temperature (25 °C) render it more suitable for environmental remediation than free laccase (pH 4.0 and 45 °C). Furthermore, the assembled laccase maintained 95.9% activity after storage for 30 days (Fig. 2d), significantly

https://doi.org/10.1038/s41467-025-58338-9

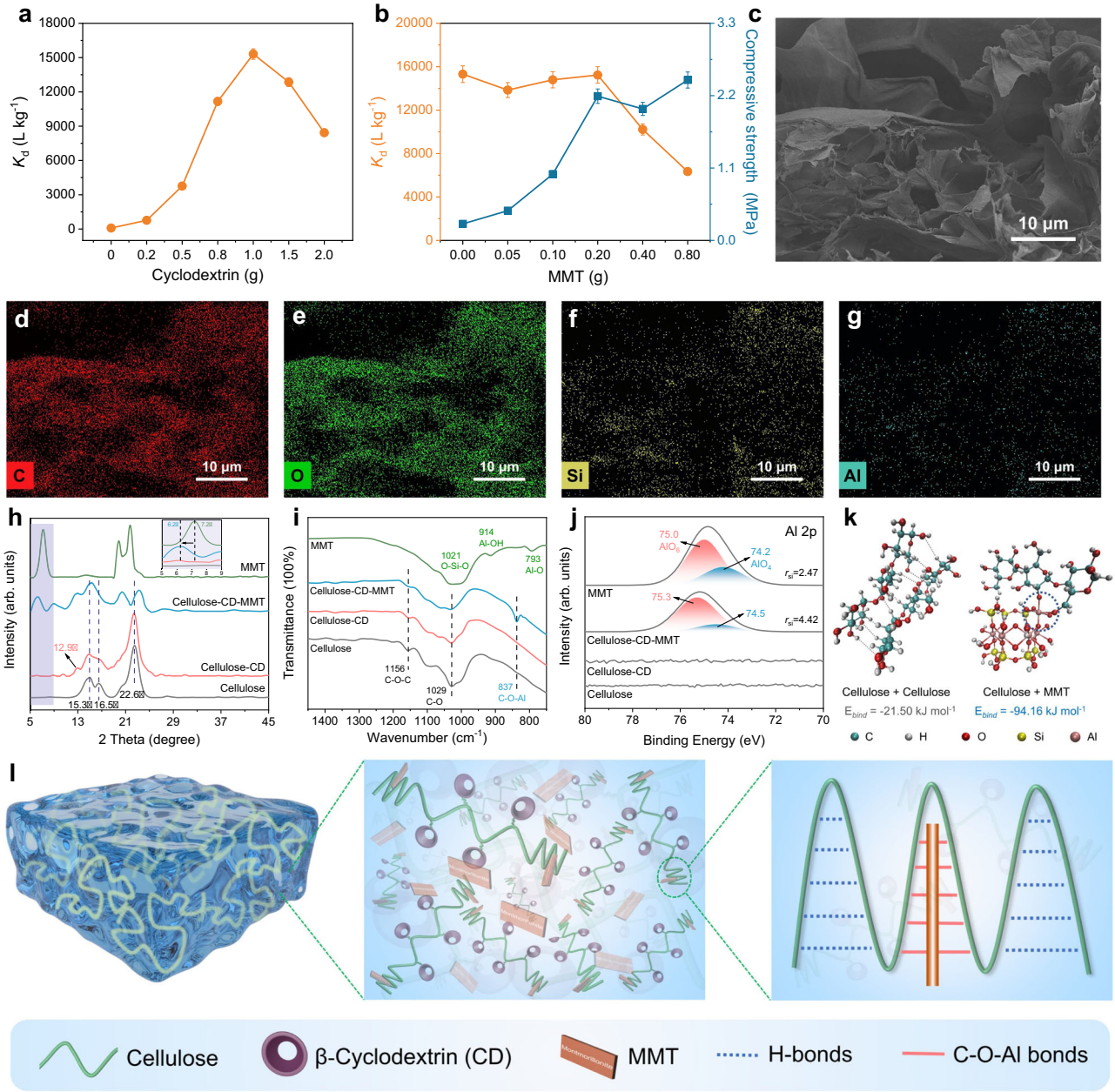

Fig. 1 | Synthesis and characterization of hydrogels. a Effect of CD doping dose on the Phe partitioning coefficient (K_d, L kg^{-1}) on the Cellulose-CD hydrogels. **b** Effects of the MMT doping dose on compressive strength of the Cellulose-CD-MMT hydrogels and the K_d of Phe on the hydrogels. The compressive strength of Cellulose-CD-MMT hydrogels increases with increasing doped amount of MMT, attributable to the exceptional mechanical strength of MMT and its abundant sites for binding to the cellulose backbone. However, excess MMT (> 0.2 g) could occupy a portion of the sites on the hydrogel for Phe sorption, thereby decreasing its K_d value to be less than 1.02×10^4 L kg^{-1} by the Cellulose-CD-MMT hydrogels. **c** FESEM image of the Cellulose-CD-MMT hydrogels. EDS mappings of C (**d**), O (**e**), Si (**f**), and Al (**g**) on the Cellulose-CD-MMT hydrogels. **h** XRD patterns of the Cellulose-, Cellulose-CD-, Cellulose-CD-MMT hydrogels, and MMT. The inset corresponds to their XRD patterns at 2θ = 5° to 9°. FTIR spectra (**i**) and Al 2p XPS spectra (**j**) of the Cellulose-, Cellulose-CD-, Cellulose-CD-MMT hydrogels, and MMT. Here, r_{si} represents the AlO_6/AlO_4 signal intensity ratio. Theoretically, the crystalline structure of MMT is formed by the coordination between AlO_6 and SiO_4 (tetrahedrally coordinated silicon); however, the facile isomorphic substitution between Si and Al results in MMT containing both AlO_6 and AlO_4 species. **k** Energy-optimized geometries and binding energy (E_{bind}, kJ mol^{-1}) of cellulose and cellulose (H-bond interaction), cellulose and MMT (coordination) via DFT calculation. **l** Schematic diagram of the proposed microstructure of the Cellulose-CD-MMT hydrogels. For (**a**, **b**), data are presented as mean ± S.D. from three replicates (n = 3).

higher than free laccase (57.0%); even after 7 cycles, it still retained 95.2% activity with 724.1 mg g^{-1} loading (Fig. 2e). As reported, immobilized enzymes have several inherent shortcomings, including steric hindrance from carriers that may disannul some active sites on the enzymes, as well as the loss of flexibility to bind ligands during degradation[18]. These limitations are directly responsible for affinity reduction of the immobilized enzyme towards reactant (i.e., higher Michaelis constant: K_m values than free enzymes)[33]. A comparison of the oxidation kinetics parameters demonstrates that the assembled laccase has a greater affinity for the substrate (2,2′-azino-bis-(3-ethylbenzothiazoline-6-sulphonic acid), ABTS) (K_m: 0.2876 mmol L^{-1}, Fig. 2f) and reaction rate (υ_{max}: 0.4467 μmol L^{-1} min^{-1}) than the free laccase (K_m: 0.6715 mmol L^{-1}, υ_{max}: 0.3753 μmol L^{-1} min^{-1}), obviously overcoming the two challenges. This can be attributed to the combined effects of the following factors: (1) CD captures substrate ABTS and facilitates access to active sites, and the rate-limiting step is primarily the substrate

https://doi.org/10.1038/s41467-025-58338-9

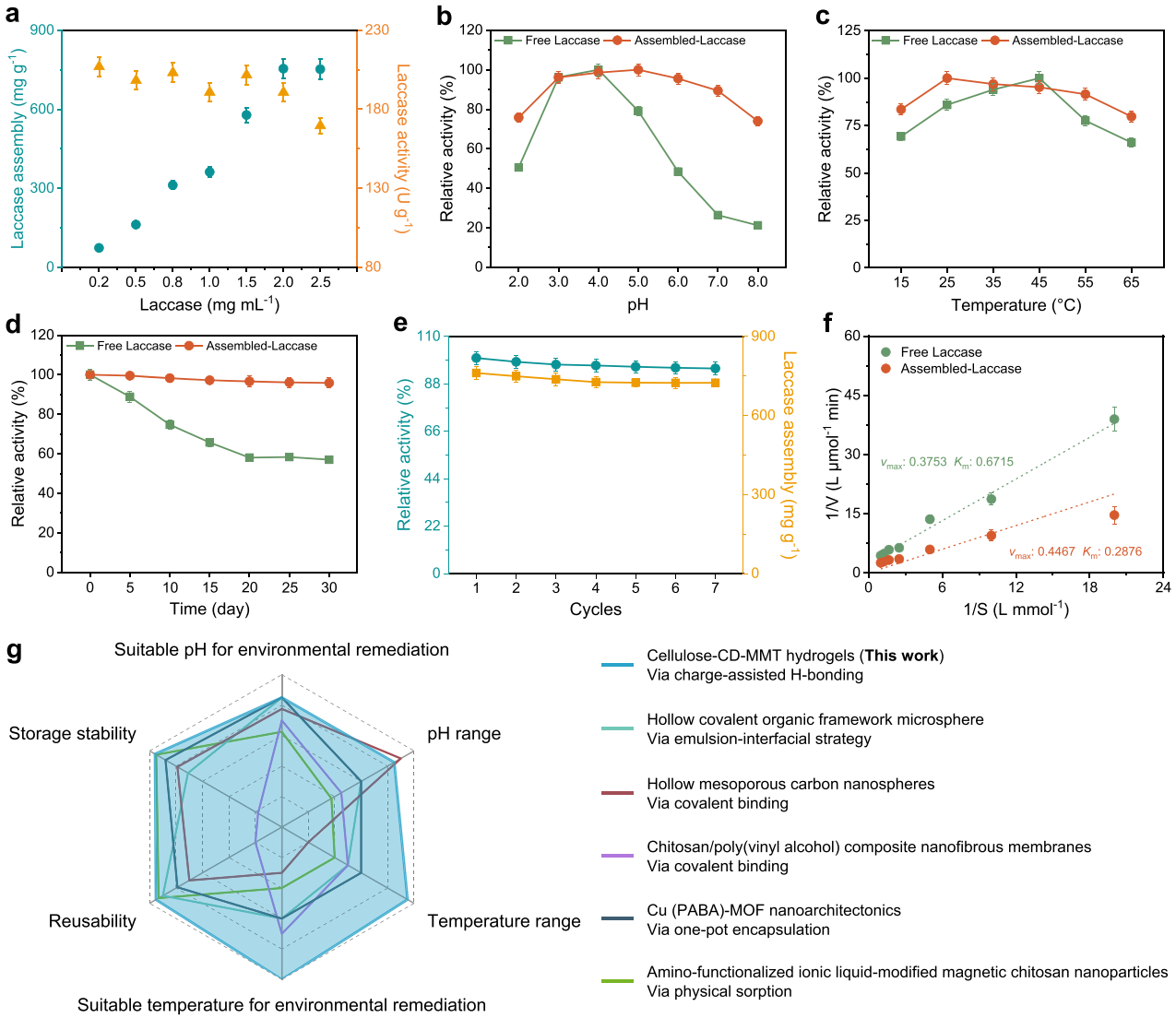

Fig. 2 | Performance and enzymatic activity stability of laccase assembled on Cellulose-CD-MMT hydrogels. a Assembled amount (mg g^{-1}) and activity (U g^{-1}) of laccase on Cellulose-CD-MMT hydrogels at different concentrations. The assembled amount of laccase on Cellulose-CD-MMT hydrogels increased with increasing laccase concentration, reaching a maximum loading of 754.5 mg g^{-1} at 2.0 mg mL^{-1}. Laccase activity sharply declined when the concentration exceeded 2.0 mg mL^{-1}, attributable to the steric hindrance caused by excess enzyme, which altered conformation and hindered substrate binding. To balance enzyme assembly capacity and activity, the Cellulose-CD-MMT hydrogels assembled with laccase at 2.0 mg mL^{-1} were utilized for the subsequent stability and degradation assays. pH (**b**), temperature (**c**), and storage (**d**) stability of free- and assembled laccase. **e** Cyclic operation and assembly stability of the assembled laccase. **f** Lineweaver-Burk plots of free- and assembled laccase. v_{max} (μmol L^{-1} min^{-1}) represents the maximum reaction rate of laccase. K_m (mmol L^{-1}) represents the Michaelis constant. A lower K_m means that the assembled enzyme requires a lower substrate concentration to achieve v_{max} and usually suggests higher affinity for the substrate. A larger value of K_m and v_{max} indicates lower affinity and higher reaction rate with substrate, respectively. The immobilized enzymes have several inherent shortcomings, including steric hindrance from carriers that may disannul some active sites on the enzymes, as well as the loss of flexibility to bind ligands during degradation. These limitations are directly responsible for the affinity reduction of the immobilized enzymes towards reactant (i.e., higher Michaelis constant: K_m values than free enzymes). **g** A comprehensive comparison between assembly strategy of laccase on Cellulose-CD-MMT hydrogels in this work and the immobilization methods of laccase on various carriers (such as nano and porous materials) in previous reports in terms of operational range of pH and temperature (maintaining in excess of 80% of enzymatic activity), suitable pH and temperature for environmental remediation, storage stability (14–30 days), and reusability (7 cycles). For (**a**–**f**), data are presented as mean ± S.D. from three replicates ($n = 3$).

diffusion (Supplementary Fig 13); (2) resemblance of hydrogels (as soft materials) to the natural extracellular matrix enabled the laccase structure to dynamically adapt and optimize its 3D conformation and activity[10,13] (Supplementary Fig. 14, Supplementary Table 4); (3) the hydrogels have a highly porous and well-dispersed network structure, minimizing steric hindrance by providing assembly binding sites for enzymes while ensuring sufficient spatial separation between immobilized enzymes to prevent crowding effects that could hinder enzymatic activity; (4) the distinct interaction (i.e., CAHB, discussed in details later) between laccase and hydrogels protects the enzyme 3D conformation (Supplementary Fig. 14) due to its moderate strength compared to strong covalent bonds, promoting adaptability, reducing steric constraints, and maintaining enzyme flexibility. These mechanisms collectively led to activity enhancement and conformation protection of the assembled laccase; meanwhile, the laccase-assembled hydrogels retained excellent activity in the presence of various interfering substances (Supplementary Fig. 15), primarily due to the protective physical barrier provided by the hydrogels, the stabilizing effect of CAHB on enzyme conformation, and the effective isolation of interfering substances through hydrogel components (CD, cellulose),

https://doi.org/10.1038/s41467-025-58338-9

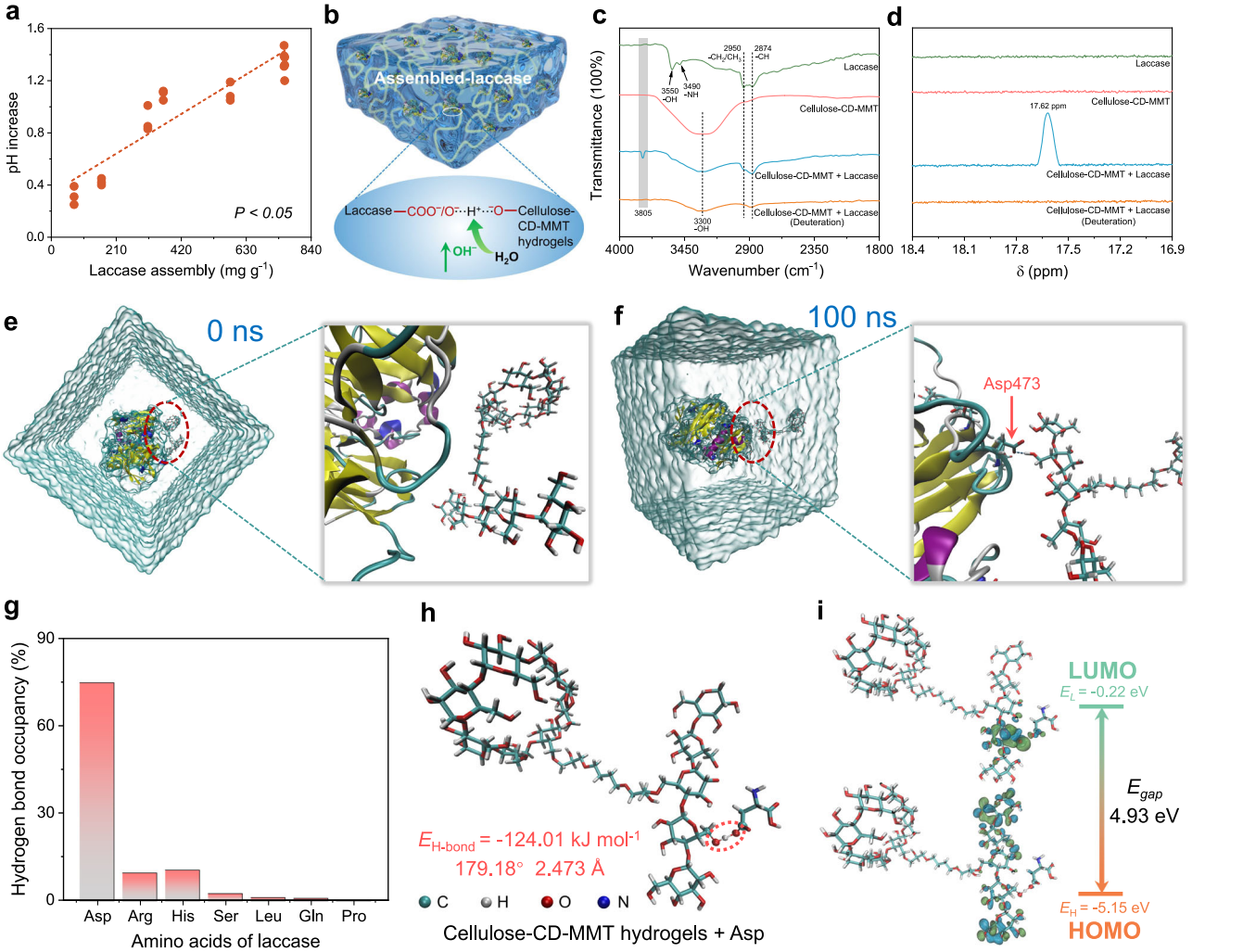

Fig. 3 | Assembling mechanism of laccase on Cellulose-CD-MMT hydrogels via CAHB. a The relationship between assembled amount of laccase on Cellulose-CD-MMT hydrogels and solution pH. The solution pH before and after laccase assembly showed that it significantly and linearly increased with increasing assembled amount of laccase ($p < 0.05$). **b** Schematic diagram of the proposed CAHB interaction between laccase and Cellulose-CD-MMT hydrogels. FTIR (**c**) and ^{1}H NMR (**d**) spectra of laccase before and after assembly (including deuteration) on Cellulose-CD-MMT hydrogels. Initial state (**e**, 0 ns) and equilibrium state (**f**, 100 ns) of the interaction between Cellulose-CD-MMT hydrogels and laccase by molecular dynamics (MD) simulation. The cyan box is a cube water box of 10 × 10 × 10 nm. **g** Contribution of different amino acids to H-bond formation between laccase and Cellulose-CD-MMT hydrogels within 100 ns MD simulation. Aspartic acid: Asp (75.02%), Arginine: Arg (9.07%), Histidine: His (10.64%), Serine: Ser (2.54%), Leucine: Leu (1.18%), Glutamine: Gln (0.91%), Proline: Pro (0.04%). Strength (**h**, $E_{H\text{-bond}}$, kJ mol^{-1}) and stability (**i**, E_{gap}, eV) of the H-bond between Cellulose-CD-MMT hydrogels and Asp quantified through DFT calculation. The representative H-bond conformation is obtained by MD simulation at 100 ns. A shorter bond length with larger bond angle and binding energy means a stronger H-bond. E_{HOMO} and E_{LUMO} are the energy (eV) of the highest occupied molecular orbital (HOMO) and lowest unoccupied molecular orbital (LUMO), respectively.

which could be important for POPs degradation. Importantly, the laccase-assembled hydrogels demonstrated improved comprehensive performance compared to the immobilized laccase on various nano or porous materials (Fig. 2g) and hydrogel-like materials (Supplementary Fig. 16) by other methods in previous reports (Supplementary Table 5).

The assembly mechanism of laccase onto Cellulose-CD-MMT hydrogels could involve electrostatic interactions, hydrogen bonding, hydrophobic interactions, van der Waals forces, and geometric matching. Since the laccase-assembled Cellulose-CD-MMT hydrogels are primarily composed of polysaccharides and laccase that consist of highly hydrophilic amino acids, hydrophobic interactions are unlikely to be the main mechanism for extensive laccase assembly. Given that laccase and Cellulose-CD-MMT hydrogels are negatively charged at pH 5.0, they would electrostatically repel each other (Supplementary Fig. 17), which is obviously not conductive to stable assembly and high activity. Additionally, other physical interactions (e.g., van der Waals forces) and geometric matching are generally insufficient to overcome the electrostatic repulsion between the hydrogels and laccase. Hence, other forces must drive the observed interactions. Given this, it is most likely that strong CAHB occurring under the condition of $|\Delta PZC| < \sim 5.0$ serves as the dominant driving force for the interaction between laccase and Cellulose-CD-MMT hydrogels, as the $|\Delta PZC|$ between them is 0.51[20,22].

The solution pH significantly and linearly increased with increasing assembled laccase amount ($p < 0.05$) due to the release of OH^- during CAHB formation, given the involvement of H^+ from the solvent H_2O in this process (Fig. 3a, b)[20,23]. Moreover, additional peaks appeared on the FTIR spectra of Cellulose-CD-MMT hydrogels at high frequencies (3805 cm^{-1}, blue shift of –OH at 3300 cm^{-1}, Fig. 3c) and in the significantly low-field region of their ^{1}H NMR spectra (17.62 ppm, Fig. 3d) after assembling laccase, which is indicative of CAHB formation[34,35]. Interestingly, the peaks belonging to CAHB disappeared after the solvent (H_2O) was replaced with D_2O (deuteration), strongly implicating H_2O involvement in CAHB formation. Importantly, similar

results were also observed in assembly of enzymes (i.e., catalase, lipase) in other fields (cosmetic therapy, food manufacturing), as well as that of another laccase (from *Aspergillus*) (Supplementary Figs. 18–21, Supplementary Table 6). These findings collectively demonstrate the CAHB, as an effective and extendable approach, effectively facilitate enzyme assembly on the Cellulose-CD-MMT hydrogels while preserving biological function.

Binding sites on laccase and CAHB intensity

To investigate the binding sites on laccase and mechanisms involved in CAHB formation at molecular level, molecular dynamics (MD) simulation and DFT calculations were performed. H-bonds were established between –OH groups on cellulose chains of Cellulose-CD-MMT hydrogels and –COOH groups on Aspartic acid (Asp) 473 of laccase at 100 ns equilibrium (Fig. 3e, f, Supplementary Fig. 22). Further analysis of the contributions from different amino acids to H-bond formation in the laccase-assembled Cellulose-CD-MMT hydrogels indicated that Asp contributed the largest fraction (75.02%, Fig. 3g), which is over 3.0-fold greater than the combined contributions from all other amino acids. This can be attributed to strong CAHB formation (hydrogels–$O^{-}\cdots H^{+}\cdots{}^{-}OOC$–laccase, −124.01 kJ mol^{-1}) between –COOH groups on Asp and the –OH groups on Cellulose-CD-MMT hydrogels (|ΔPZC| = 1.37, Fig. 3h, Supplementary Fig. 23)[22,36]. Conversely, weaker ordinary H-bonds were created between Cellulose-CD-MMT hydrogels and –NH groups on Arginine (−13.57 kJ mol^{-1}, Supplementary Fig. 24) or Histidine (−14.82 kJ mol^{-1}) given their high |ΔPZC| (8.67 or 9.36), thereby contributing to a small fraction. Meanwhile, CAHB exhibited a greater E_{gap} value (4.93 eV) compared to the ordinary H-bond (≤ 3.20 eV), demonstrating its higher stability (Fig. 3i, Supplementary Table 7). In addition, unlike Asp, Arg, and His, the remaining four amino acids (Serine, Leucine, Glutamine, Proline) in laccase are of neutral charge, and only form ordinary H-bonds with Cellulose-CD-MMT hydrogels[22]. These analyses demonstrate that the stronger and more stable CAHB (weaker than covalent bonds that typically impede enzyme flexibility) was formed between Cellulose-CD-MMT hydrogels and Asp, resulting in stable laccase assembly (Supplementary Fig. 25), enzymatic activity enhancement and conformation protection. Similar CAHB formation also occurred between laccase and Cellulose-CD- and Cellulose hydrogels (Supplementary Figs. 26, 27). The unobserved potential CAHB formation between glutamic acid in laccase and hydrogels (Fig. 3g and Supplementary Fig. 26g) may be due to the limited amount of glutamic acid, steric hindrance, and competitive interactions (Supplementary Fig. 28). These results hold potential significance for designing other biodegradation agents and programmable modification of protein function.

Contaminants removal by the laccase-assembled hydrogels

The contaminant removal performance of the laccase-assembled Cellulose-CD-MMT hydrogels was assessed using three PAHs (i.e., naphthalene: Nap; phenanthrene: Phe; and pyrene: Pyr) as representative POPs. These PAHs are common contaminants found in polluted media such as coking wastewater, groundwater and even Antarctica[37–39]. The total removal (a sum of sorption and degradation) and net degradation efficiency of three PAHs at 10, 80, 120 μg L^{-1} by the laccase-assembled Cellulose-CD-MMT hydrogels were 95.9–99.2% and 68.2–85.0%, respectively (Fig. 4a), significantly exceeding that of free laccase (20.5–47.6%). This enhanced removal can be attributed to the accumulation of CD and degradation by the assembled laccase with increased enzymatic activity, electron transfer rate and apparent redox potential (Supplementary Figs. 29, Supplementary Table 8). In addition, the degradation rates of Nap (0.104 μg h^{-1}), Phe (0.098 μg h^{-1}), and Pyr (0.097 μg h^{-1}) by the assembled laccase within 0–12 h were 3.06-, 3.38- and 6.93-times that of free laccase, respectively (Fig. 4b). Importantly, after undergoing 10 cycles, the laccase-assembled hydrogels still maintained > 91.7% total removal and > 67.5% net degradation efficiency (Fig. 4c, Supplementary Fig. 30). Emphatically, the laccase-assembled hydrogels also exhibited excellent total removal (> 90.9%) and degradation (> 83.7%, using redox mediator) efficiency for removing other organic pollutants of regulatory or popular concerns like perfluorooctanoic acid, perfluorooctanesulfonic acid, sulfamethoxazole, and ciprofloxacin (Supplementary Fig. 31), demonstrating a great potential in environmental remediation of diverse emerging organic pollutants.

The environmental applicability of the laccase-assembled hydrogels to remove these PAHs at different pHs and in the presence of coexisting anions/cations, heavy metals, organic contaminants (perfluorooctanesulfonic acid), and dissolved organic matter (humic acid) was examined (Supplementary Figs. 32 and 33). These conditions and agents had no significant effect (< 6.84% for all cases) on the removal and degradation of the PAHs by the laccase-assembled hydrogels, while free laccase showed significantly reduced efficiency under these conditions (up to 39.34%, Supplementary Fig. 34). Importantly, the laccase-assembled hydrogels achieved > 80.4% total removal and > 62.0% degradation of 16 USEPA priority PAHs from Coal Chemical Plant wastewater (Ningxia, China), which was 21.77–62.28 and 19.61–52.34 times that of free laccase (Supplementary Figs. 35, 36, Supplementary Tables 9, 10), respectively. The abovementioned enhanced performances are better than most reported approaches or materials (Supplementary Table 11). Notably, both removal (each > 77.1%) and degradation (each > 60.0%) efficiencies remain high in a larger real wastewater system (500 mL) (Supplementary Figs. 37). These findings highlight the high environmental applicability (robustness), reusability, and practical remediation performance of the laccase-assembled Cellulose-CD-MMT hydrogels, attributed to the enhanced stability and activity of laccase and strong mechanical strength of the internal structure.

The degradation pathways and mechanisms of PAHs removal by the assembled laccase were investigated using DFT calculations to predict vulnerable sites on the contaminant molecules, and gas chromatography-mass spectrometry to identify degradation intermediates. The laccase-mediated degradation mechanism involves a single-electron redox reaction[40,41] (Fig. 4d), targeting PAHs sites most likely to lose electrons. Specifically, the degradation process can be divided into three steps: (1) PAHs were degraded by oxidization near the T1 copper center of laccase and released electrons; (2) The electrons were subsequently transferred to a trinuclear copper cluster site that contained T2 and T3 copper centers via the Histidine-Cysteine-Histidine (His-Cys-His) tripeptide pathway within laccase; (3) O_2 molecules near the trinuclear copper cluster site accepted electrons and were reduced to H_2O. Figure 4e illustrates the Phe molecular structure with labeled atomic positions, the HOMO, and the distribution of electrophilic (f_A^-) attacking sites based on compressed Fukui function by DFT calculation. The f_A^- values for each atom in Phe molecule are presented in Supplementary Table 12. The greatest f_A^- (0.0977) values are at C5 and C6 with plenty of HOMO, indicating a ready loss of electrons and subsequent bond breaking and oxidation[42,43]. The identified degraded products suggest a possible degradation pathway starting from attack at C5 and C6 (Supplementary Fig. 38, Fig. 4f), generating phenanthrene-9,10-diol (P1), followed by conversion to phenanthrene-9,10-dione (P2), then to diphenic acid (P3) through ring-opening reactions, and then to phthalic acid (P4) and either 1,2-benzoquinone or 1,4-benzoquinone (P5 or P6) via oxidation and tautomerism processes. Finally, P5 or P6 were mineralized to the inorganic products CO_2 and H_2O. Nap (Supplementary Figs. 39–40, Supplementary Table 13) and Pyr (Supplementary Figs. 41–43, Supplementary Table 14) followed similar degradation pathways as they are congeners. The acute toxicity (i.e., *Daphnia magna* -$Log_{10}^{(48\ h\ LC50)}$) and bioconcentration factor of Nap, Phe, Pyr, and their intermediates were evaluated, showing that degraded products of the three PAHs largely exhibit lower acute toxicity and bioconcentration levels than

https://doi.org/10.1038/s41467-025-58338-9

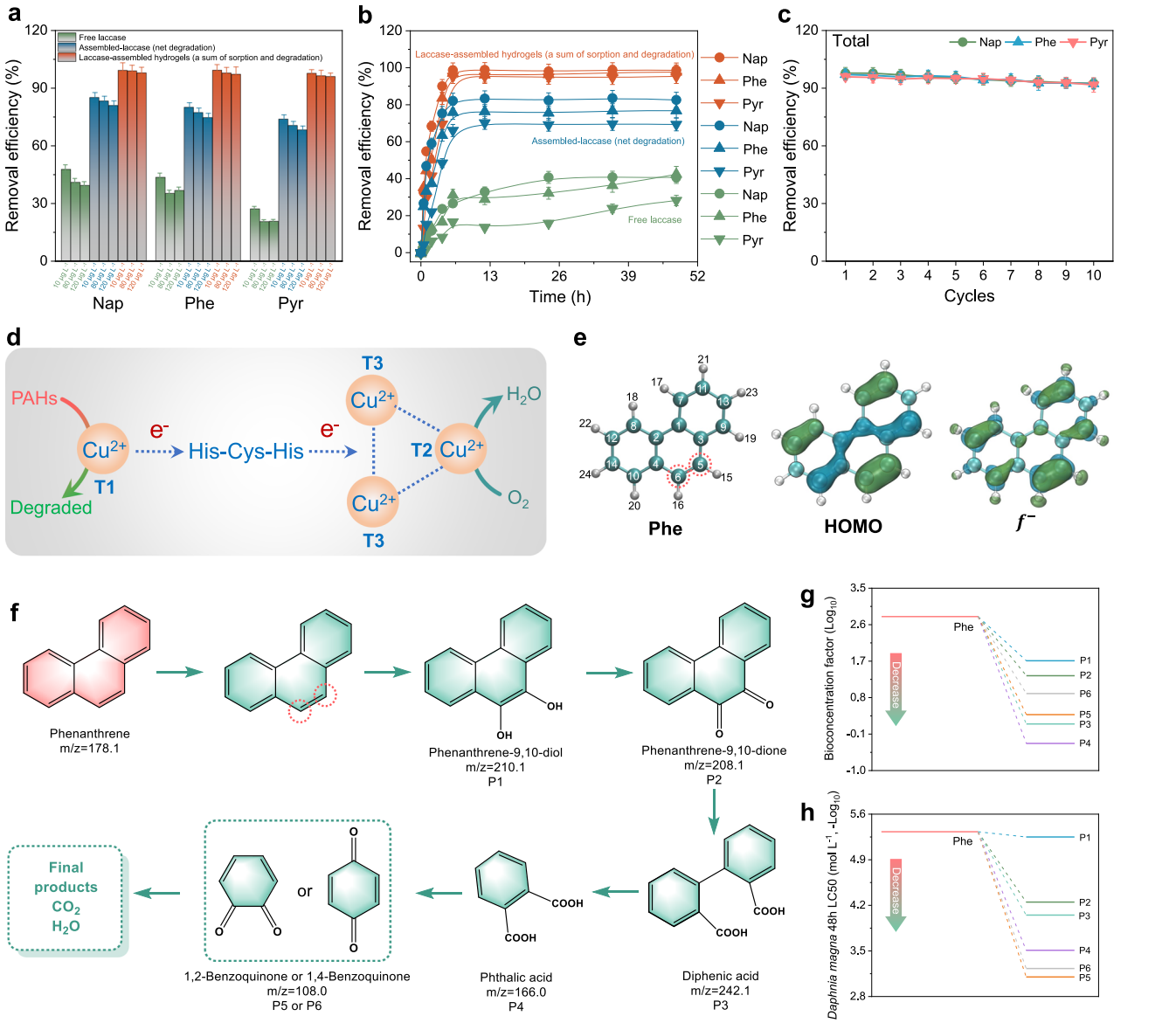

Fig. 4 | Removal performance and reusability of the laccase-assembled Cellulose-CD-MMT hydrogels, as well as degradation mechanisms and pathways of PAHs. a Removal efficiency of Nap, Phe, and Pyr at 10, 80, 120 μg L^{-1} by the laccase-assembled Cellulose-CD-MMT hydrogels (a sum of sorption and degradation), assembled laccase (net degradation), and free laccase. The net degradation efficiency of PAHs by the assembled laccase was investigated by inactivated assembled laccase as the control. Degradation of the three PAHs by the assembled- and free laccase followed the order Pyr < Phe < Nap, which aligns with the chemical stability increases with increasing benzene ring number, thereby decreasing degradability. **b** Removal kinetics of PAHs (80 μg L^{-1}) by the laccase-assembled Cellulose-CD-MMT hydrogels (a sum of sorption and degradation), assembled laccase (net degradation), and free laccase. Degradation efficiency of three PAHs by free laccase within 48 h was below 42.4%. This could be attributed to limited diffusion of the substrate PAHs, low substrate concentration near the laccase active site, and limited redox potential and electron transfer rate, resulting in limited reaction between the substrate and enzyme. Conversely, equilibrium for the net degradation of the PAHs by the assembled laccase was reached within 12 h. **c** Reusability of the laccase-assembled Cellulose-CD-MMT hydrogels for removal of PAHs (80 μg L^{-1}), and the hydrogels were recycled 10 times. **d** Degradation mechanism of PAHs by the assembled laccase. **e** Phe molecular structure with labeled atomic positions, the HOMO of Phe, and the distribution of electrophilic (f_A^-) attacking sites based on compressed Fukui function (CFF). **f** Proposed degradation pathways of Phe by the assembled laccase. Bioconcentration factor (**g**, BCF, Log_{10}) and acute toxicity (**h**, *Daphnia magna* 48 h LC50, -Log_{10}, mol L^{-1}) of Phe and its intermediates via the Toxicity Estimation Software Tool (T.E.S.T. 5.1.2). For (**a**–**c**), data are presented as mean ± S.D. from three replicates ($n = 3$).

the associated parent compounds (Fig. 4g, h, Supplementary Fig. 44). Importantly, the laccase-assembled Cellulose-CD-MMT hydrogels showed no significant toxicity (24 h and 48 h) to L929 mouse fibroblast cells at 6–15 mg mL^{-1} (Supplementary Fig. 45), indicating a high degree of biocompatibility.

Discussion

Immobilizing enzymes on hydrogels, particularly biopolymer cellulose-based hydrogels, holds promise in addressing limitations in enzyme-catalyzed bioremediation, such as high cost, lack of robustness, and low recyclability. However, challenges, including low enzyme loading, limited activity/stability, poor affinity for POPs, low mechanical strength, limited redox potential and electron transfer rate, still remain. Herein, Cellulose-CD-MMT hydrogels with high affinity for POPs and exceptional mechanical strength were fabricated, and subsequently assembled laccase (754.5 mg g^{-1}) using an advanced and scalable strategy (CAHB). The advanced laccase-assembled hydrogels overcome the aforementioned challenges, and exhibited high

efficiency (> 90.9%) at removing diverse organic pollutants including antibiotics, PFAS and PAHs, and excellent reusability, overmatching most other reported approaches or materials. Importantly, the laccase-assembled hydrogels demonstrated high performance in wastewater treatment, with an overall removal efficiency and net degradation efficiency for 16 USEPA priority PAHs that was 21.77–62.28 times and 19.01–52.34 times that of free laccase. This work not only provides an alternative perspective for the enzyme immobilization with enhanced activity/stability and for the preparation of multi-enzyme co-immobilization strategy, but also demonstrates great potential use in diverse fields such as drug delivery and biosensing.

Methods

Reagents and chemicals

Cellulose with a polymerization degree of 610 was purchased from Hubei Jinhanjiang Refined Cotton Co., Ltd (China). β-cyclodextrin (CD, ≥ 99%) was obtained from Beijing Xinhengyan Technology Co., Ltd. (China). 1,4-butanediol diglycidyl ether (BDE, ≥ 99%) was provided by Shanghai Macklin Biochemical Co., Ltd. (China). Laccase from *Trametes versicolor* (≥ 95%), Lipase (≥ 95%), Catalase (≥ 95%) and 2,2′-azino-bis-(3-ethylbenzothiazoline-6-sulphonic acid) (ABTS, ≥ 99%) were purchased from Shanghai Yuanye Bio-Technology Co., Ltd. (China). Laccase from *Aspergillus* (≥ 95%) was provided by Beijing Psaitong Biotechnology Co., Ltd. (China). Montmorillonite (≥ 99%) was obtained from Adamas Reagent Co., Ltd. (China), and subsequent nanosheets (MMT) were prepared by a mechanical exfoliation method[27]. Specifically, montmorillonite powder (6 g) was dispersed in deionized water (1 L) under continuous stirring for 7 days. The suspension was then centrifuged twice at 1100 × *g* for 10 min to remove unexfoliated aggregates. The resulting transparent supernatant, which exhibited stability for over a week, was collected and dried to yield MMT. PAHs (naphthalene: Nap; phenanthrene: Phe; and pyrene: Pyr ≥ 99%) were purchased from TCI Development Co., Ltd. (Japan). Pentadecafluorooctanoic acid (PFOA, ≥ 98%) was obtained from Shanghai Aladdin Reagent Co. Ltd. (China). Perfluorooctanesulfonic acid (PFOS, ≥ 96%) was obtained from Cayman Chemical Company (USA). Sulfamethoxazole (SMX ≥ 98%) and ciprofloxacin (CIP ≥ 98%) were purchased from Sigma-Aldrich (USA). All other chemicals and reagents used (Urea, NaOH, HCl, KH_2PO_4, KD_2PO_4, NaOD, DCl) are of analytical grade.

Synthesis of Cellulose-, Cellulose-CD-, and Cellulose-CD-MMT hydrogels

A cellulose solution (3 wt%) was prepared by dissolving the biopolymer in a mixed solution (97 g) that contained urea (12 wt%) and NaOH (7 wt%) at -12 °C[44]. The cross-linker 1,4-butanediol diglycidyl ether (BDE, 5.0 g) was then added to the cellulose solution for homogeneous mixing. The mixture was centrifugally degassed at 1900 × *g* for 20 min, and then transferred to a mold and maintained at 45 °C for 6 h to induce hydrogel formation. The hydrogels were then immersed in a 75% ethanol solution for 6 h and then washed with DI-water for 3 days to remove excess impurities to prepare Cellulose hydrogels.

To dope CD onto the Cellulose hydrogels and determine the optimal dose of PAHs capture, varying amounts of CD (0–2.0 g) were added to the cellulose solution (3.0 wt%) that contained 5.0 g of the cross-linker BDE. The optimum CD dose for preparation of CD-doped Cellulose hydrogels (Cellulose-CD) was 1.0 g (Fig. 1a). Cellulose-CD hydrogels prepared with the optimal doped dose of CD were collected for the subsequent characterizations. MMT was added to increase the hydrogel mechanical strength; specifically, different amounts of MMT (0–0.8 g) were mixed with 1.0 g CD and 5.0 g BDE in the cellulose solution (3.0 wt%) to determine the optimal dose. The optimum dose of MMT was 0.2 g. The final Cellulose hydrogels with CD and MMT doped exhibited high mechanical strength (Fig. 1b). Based upon above, the final Cellulose-CD-MMT hydrogels, mainly present in the form of cylindrical particles with a diameter of ~0.2 cm and height of ~0.2 cm, were synthesized with 1.0 g CD, 0.2 g MMT, and 5.0 g BDE in the 3.0% cellulose solution.

Assembly of laccase on Cellulose-CD-MMT hydrogels

To assemble laccase on Cellulose-CD-MMT hydrogels, 90 mg of hydrogels were added to 40 mL of phosphate buffer solution (KH_2PO_4, pH 5.0) that contained different concentrations of laccase (0–2.5 mg mL^{-1}) (Supplementary Table 15). The mixture was shaken for 24 h in the dark at 180 rpm and 25 °C. Our preliminary test showed that this time was sufficient to reach equilibrium for laccase assembly (Supplementary Fig. 46). After centrifuging the mixture at 1900 × *g* for 20 min, the supernatant was collected, and the laccase content was determined by the Bradford method at 595 nm (Supplementary Note 2)[45]. The laccase-assembled Cellulose-CD-MMT hydrogels were thoroughly rinsed with phosphate buffer solution, and then sealed and stored at 4 °C for later use. A laccase enzymatic activity assay was performed using the ABTS method at 420 nm[46]; the oxidation kinetics of the substrate (ABTS) by both free- and assembled laccase was determined at 0.05–1.0 mmol L^{-1} (see Supplementary Note 3 for details). To evaluate the stability of free- and assembled laccase, a series of stability experiments, including varying pH and temperature, reusability, storage- and assembly stability, were conducted (Supplementary Note 4).

Sample characterization

To clarify the formation and physicochemical properties of hydrogels (i.e., Cellulose, Cellulose-CD and Cellulose-CD-MMT), as well as the immobilizing mechanism of laccase on Cellulose-CD-MMT hydrogels, the following characterization techniques were used. The surface morphology and elemental composition of the Cellulose-CD-MMT hydrogels were determined by a field-emission scanning electron microscope coupled with an energy dispersive spectrometer (FESEM-EDS, Merlin Compact, Zeiss, Germany). N_2 sorption-desorption isotherms on the Cellulose-CD-MMT hydrogels at 77 K were obtained using a surface area analyzer (ASAP 2020 HD88, Micromeritics, USA); hydrogels specific surface area and pore diameter distribution were calculated using Brunauer-Emmett-Teller (BET) and Barrett-Joyner-Halenda (BJH) methods, respectively. The functional groups on the laccase-assembled Cellulose-CD-MMT hydrogels before and after H/D isotope replacement, as well as free laccase and all other preliminary hydrogels, were characterized by an attenuated total reflection-Fourier transform micro infrared spectrometer (ATR-FTIR, Spotlight 200, PerkinElmer, USA) from 400 to 4000 cm^{-1}. The crystalline structure of hydrogels, and zeta potential of hydrogels and laccase were measured by a powder X-ray diffractometer (XRD, Empyrean, Panalytical, Netherlands) in the diffraction angle (2θ) ranging from 3° to 70° and a Nanosizer (Nano-ZS90, Malvern Panalytical, UK), respectively. The surface chemical composition and the elemental binding energy of all hydrogels were measured by an X-ray photoelectron spectrometer (XPS, Kratos AXIS Ultra DLD, Shimadzu, Japan). The compression properties of the Cellulose-CD and Cellulose-CD-MMT hydrogels were measured using a universal testing machine so as to understand how MMT doping enhanced mechanical strength of the Cellulose-CD hydrogels (CMT 6103, MTS, China). The details for compression property measurement are described in Supplementary Note 5. The immobilization images of the laccase-labeled with FITC on Cellulose-CD-MMT hydrogels were acquired by confocal laser scanning microscopy (CLSM, A1Rsi, Nikon, Japan). The conformation of laccase was detected by a circular dichroism spectrometer (J-1500, JASCO, Japan) and ATR-FTIR. To verify whether charge-assisted hydrogen bonds (CAHB) were formed between the Cellulose-CD-MMT hydrogels and laccase, the H/D isotope tracer method was applied using D_2O and KD_2PO_4 instead of H_2O and KH_2PO_4 as solvents (Supplementary

Note 5); additional procedures were identical to those for laccase assembly as described above. Prior to test, the laccase-assembled Cellulose-CD-MMT hydrogels were freeze-dried for 24 h and then ground to powder. The powders were then analyzed by liquid-state ^{1}H nuclear magnetic resonance spectrometry (^{1}H NMR, Avance NEO 600, Bruker, Germany).

Contaminant removal

The removal of Nap, Phe and Pyr at realistic environmental concentrations (10–120 μg L^{-1}) by hydrogels, free laccase and laccase-assembled Cellulose-CD-MMT hydrogels (including those assembled with inactivated laccase) was investigated in 15 mL glass vials at 180 rpm and 25 °C (Supplementary Note 6). The dose of free laccase was the same as that of laccase contained in the laccase-assembled hydrogels. The degradation efficiency of PAHs by the assembled laccase was calculated by the difference of the total removal efficiency of PAHs by laccase-assembled hydrogels (sorption and degradation) and that by the hydrogels assembled with inactivated laccase (only sorption). The concentration of PAHs in the aqueous phase was determined by ultra-high performance liquid chromatography (UHPLC, LC-20A, Shimadzu, Japan). The degradation products of PAHs were analyzed by gas chromatography-mass spectrometry (GC-MS, 7890A-5975C, Agilent, USA). The details for PAHs removal experiment, as well as the UHPLC and GC-MS analysis conditions, are all described in the Supplementary Information (Supplementary Notes 6–8, Supplementary Fig. 47). The reusability and robustness of the laccase-assembled Cellulose-CD-MMT hydrogels for PAHs removal were evaluated over 10 cycles. In addition, the removal of other organic pollutants of regulatory or emerging concern including perfluorooctanoic acid, perfluorooctanesulfonic acid, sulfamethoxazole, and ciprofloxacin were also investigated (Supplementary Note 6). This removal experiment used the 16 USEPA priority PAHs, including naphthalene (Nap), acenaphthylene, acenaphthene, fluorene, phenanthrene (Phe), anthracene, fluoranthene, pyrene (Pyr), benzo(*a*)anthracene, chrysene, benzo(*b*)fluoranthene, benzo(*k*)fluoranthene, benzo(*a*)pyrene, dibenzo(*a,h*)anthracene, indeno(*1,2,3-cd*)pyrene, and benzo(*g,h,i*)perylene from an authentic wastewater sample from a Coal Chemical Plant in Ningxia, China. Additional experimental details are in the Supplementary Note 6.

MD simulation and DFT calculations

MD simulation was performed with the software package GROMACS 2020.6[47] to discover the H-bond sites between Cellulose-CD-MMT hydrogels and laccase. The laccase and Cellulose-CD-MMT hydrogel models were parameterized by the AMBER14SB_parmbsc1 force field and the generalized AMBER force field (GAFF), respectively. An extended simple point charge (SPC/E) water model was used. The neutralization of the simulation system was conducted by adding Na^+ or Cl^- counter ions. The simulation of the system that contained Cellulose-CD-MMT hydrogels and laccase lasted 100 ns with a time step of 2 fs. Additional details for MD simulation and the model construction for the Cellulose-CD-MMT hydrogels can be found in Supplementary Note 9 and Supplementary Figs. 48–49.

The representative H-bond conformations between Cellulose-CD-MMT hydrogels and amino acids in laccase were obtained from MD simulation. The strength and stability of different H-bonds were calculated by DFT using Gaussian 16 software package[48]. Geometric optimization and energy calculation were performed using B3LYP functional with the basis sets of 6-311 + G** and def2-TZVP, respectively. The DFT-D3 (BJ) dispersion correction was used. An implicit solvent using the solvation model based on density (SMD) was used, with water as the solvent. The binding energy and energy gap (E_{gap}) of different H-bonds were used to evaluate their strength and stability, respectively[36]. In addition, the sorption energy of Phe on Cellulose- and Cellulose-CD hydrogels, the binding energy between cellulose and cellulose, cellulose and MMT were calculated using the same level. The highest occupied molecular orbital (HOMO) and condensed Fukui functions of PAHs were calculated to predict the attacking sites during degradation processes[42,43]. The DFT calculation details and equations are shown in Supplementary Note 10.

Reporting summary

Further information on research design is available in the Nature Portfolio Reporting Summary linked to this article.

Data availability

All data generated or analyzed in this study are included in this published article and its Supplementary Information files. All data are available upon request. Source data are provided with this paper.

References

1. Michalak, A. M. et al. The frontiers of water and sanitation. *Nat. Water* **1**, 10–18 (2023).
2. Xu, Y. et al. Electrochemical hydrogenation of oxidized contaminants for water purification without supporting electrolyte. *Nat. Water* **1**, 95–103 (2023).
3. Li, J. et al. Sustainable environmental remediation via biomimetic multifunctional lignocellulosic nano-framework. *Nat. Commun.* **13**, 4368 (2022).
4. Somboon, K., Doble, A., Bulmer, D., Baslé, A., Khalid, S. & van den Berg, B. Uptake of monoaromatic hydrocarbons during biodegradation by FadL channel-mediated lateral diffusion. *Nat. Commun.* **11**, 6331 (2020).
5. Luo, Y. H. et al. A synergistic platform for continuous co-removal of 1,1,1-trichloroethane, trichloroethene, and 1,4-dioxane via catalytic dechlorination followed by biodegradation. *Environ. Sci. Technol.* **55**, 6363–6372 (2021).
6. Jasmann, J. R., Gedalanga, P. B., Borch, T., Mahendra, S. & Blotevogel, J. Synergistic treatment of mixed 1,4-dioxane and chlorinated solvent contaminations by coupling electrochemical oxidation with aerobic biodegradation. *Environ. Sci. Technol.* **51**, 12619–12629 (2017).
7. DelRe, C. et al. Near-complete depolymerization of polyesters with nano-dispersed enzymes. *Nature* **592**, 558–563 (2021).
8. Świderek, K. et al. Mechanistic studies of a lipase unveil effect of pH on hydrolysis products of small PET modules. *Nat. Commun.* **14**, 3556 (2023).
9. Sheldon, R. A., Basso, A. & Brady, D. New frontiers in enzyme immobilisation: robust biocatalysts for a circular bio-based economy. *Chem. Soc. Rev.* **50**, 5850–5862 (2021).
10. Wang, X. & Wang, Q. Enzyme-laden bioactive hydrogel for biocatalytic monitoring and regulation. *Acc. Chem. Res.* **54**, 1274–1287 (2021).
11. Xu, W., Jiao, L., Wu, Y., Hu, L., Gu, W. & Zhu, C. Metal–organic frameworks enhance biomimetic cascade catalysis for biosensing. *Adv. Mater.* **33**, 2005172 (2021).
12. Küchler, A., Yoshimoto, M., Luginbühl, S., Mavelli, F. & Walde, P. Enzymatic reactions in confined environments. *Nat. Nanotechnol.* **11**, 409–420 (2016).
13. Lou, J. & Mooney, D. J. Chemical strategies to engineer hydrogels for cell culture. *Nat. Rev. Chem.* **6**, 726–744 (2022).
14. Weerasundara, L., Gabriele, B., Figoli, A., Ok, Y. S. & Bundschuh, J. Hydrogels: novel materials for contaminant removal in water—a review. *Crit. Rev. Environ. Sci. Technol.* **51**, 1970–2014 (2020).

15. Gokhale, D., Hamelberg, A. F. & Doyle, P. S. Multifunctional zwitterionic hydrogels for the rapid elimination of organic and inorganic micropollutants from water. *Nat. Water* **2**, 62–71 (2024).
16. Bolivar, J. M., Woodley, J. M. & Fernandez-Lafuente, R. Is enzyme immobilization a mature discipline? Some critical considerations to capitalize on the benefits of immobilization. *Chem. Soc. Rev.* **51**, 6251–6290 (2022).
17. Li, Y.-M. et al. Fine-tuning the micro-environment to optimize the catalytic activity of enzymes immobilized in multivariate metal–organic frameworks. *J. Am. Chem. Soc.* **143**, 15378–15390 (2021).
18. Zhu, Y. et al. Continuous artificial synthesis of glucose precursor using enzyme-immobilized microfluidic reactors. *Nat. Commun.* **10**, 4049 (2019).
19. Dereka, B., Yu, Q., Lewis, N. H. C., Carpenter, W. B., Bowman, J. M. & Tokmakoff, A. Crossover from hydrogen to chemical bonding. *Science* **371**, 160–164 (2021).
20. Li, X., Pignatello, J. J., Wang, Y. & Xing, B. New insight into adsorption mechanism of ionizable compounds on carbon nanotubes. *Environ. Sci. Technol.* **47**, 8334–8341 (2013).
21. Zhao, J. et al. Homo-conjugation of low molecular weight organic acids competes with their complexation with Cu(II). *Environ. Sci. Technol.* **52**, 5173–5181 (2018).
22. Gilli, P., Pretto, L., Bertolasi, V. & Gilli, G. Predicting hydrogen-bond strengths from acid-base molecular properties. The pK_a slide rule: Toward the solution of a long-lasting problem. *Acc. Chem. Res.* **42**, 33–44 (2009).
23. Li, X., Gámiz, B., Wang, Y., Pignatello, J. J. & Xing, B. Competitive sorption used to probe strong hydrogen bonding sites for weak organic acids on carbon nanotubes. *Environ. Sci. Technol.* **49**, 1409–1417 (2015).
24. Ling, C. et al. High adsorption of sulfamethoxazole by an amine-modified polystyrene–divinylbenzene resin and its mechanistic insight. *Environ. Sci. Technol.* **50**, 10015–10023 (2016).
25. Pignatello, J. J., Mitch, W. A. & Xu, W. Activity and reactivity of pyrogenic carbonaceous matter toward organic compounds. *Environ. Sci. Technol.* **51**, 8893–8908 (2017).
26. Lu, C. & Chen, X. All-temperature flexible supercapacitors enabled by antifreezing and thermally stable hydrogel electrolyte. *Nano Lett.* **20**, 1907–1914 (2020).
27. Wang, J., Cheng, Q., Lin, L. & Jiang, L. Synergistic toughening of bioinspired poly(vinyl alcohol)-clay-nanofibrillar cellulose artificial nacre. *ACS Nano* **8**, 2739–2745 (2014).
28. Pu, Z., Huang, J., Li, J., Feng, H., Wang, X. & Yin, X. Effect of F content on the structure, viscosity and dielectric properties of SiO_2-Al_2O_3-B_2O_3-RO-TiO_2 glasses. *J. Non-Cryst. Solids* **563**, 120817 (2021).
29. Ngouana W, B. F. & Kalinichev, A. G. Structural arrangements of isomorphic substitutions in smectites: molecular simulation of the swelling properties, interlayer structure, and dynamics of hydrated Cs–montmorillonite revisited with new clay models. *J. Phys. Chem. C.* **118**, 12758–12773 (2014).
30. Chen, L. et al. Scalable production of biodegradable, recyclable, sustainable cellulose–mineral foams via coordination interaction assisted ambient drying. *ACS Nano* **16**, 16414–16425 (2022).
31. Yoosefian, M., Ansarinik, Z. & Etminan, N. Density functional theory computational study on solvent effect, molecular conformations, energies and intramolecular hydrogen bond strength in different possible nano-conformers of acetaminophen. *J. Mol. Liq.* **213**, 115–121 (2016).
32. Zhang, J. et al. A key role of inner-cation-π interaction in adsorption of Pb(II) on carbon nanotubes: experimental and DFT studies. *J. Hazard. Mater.* **412**, 125187 (2021).
33. Feng, D. et al. Stable metal-organic frameworks containing single-molecule traps for enzyme encapsulation. *Nat. Commun.* **6**, 5979 (2015).
34. Sorgenfrei, N. et al. NMR spectroscopic characterization of charge assisted strong hydrogen bonds in brønsted acid catalysis. *J. Am. Chem. Soc.* **138**, 16345–16354 (2016).
35. Zhang, J. et al. Adsorption, desorption and coadsorption behaviors of sulfamerazine, Pb(II) and benzoic acid on carbon nanotubes and nano-silica. *Sci. Total Environ.* **738**, 139685 (2020).
36. Zhang, J. et al. Direct spectroscopic evidence for charge-assisted hydrogen-bond formation between ionizable organic chemicals and carbonaceous materials. *Environ. Sci. Technol.* **56**, 9356–9366 (2022).
37. Iriarte, J., Dachs, J., Casas, G., Martínez-Varela, A., Berrojalbiz, N. & Vila-Costa, M. Snow-dependent biogeochemical cycling of polycyclic aromatic hydrocarbons at coastal Antarctica. *Environ. Sci. Technol.* **57**, 1625–1636 (2023).
38. Qiao, X., Zheng, B., Li, X., Zhao, X., Dionysiou, D. D. & Liu, Y. Influencing factors and health risk assessment of polycyclic aromatic hydrocarbons in groundwater in China. *J. Hazard. Mater.* **402**, 123419 (2021).
39. Saber, A. N., Zhang, H., Islam, A. & Yang, M. Occurrence, fates, and carcinogenic risks of substituted polycyclic aromatic hydrocarbons in two coking wastewater treatment systems. *Sci. Total Environ.* **789**, 147808 (2021).
40. Feng, Y. et al. Mechanistic insights into the biodegradation of carbon dots by fungal laccase. *Environ. Sci. Technol.* **57**, 11977–11987 (2023).
41. Xu, X. et al. A customizable 3D printed device for enzymatic removal of drugs in water. *Water Res.* **208**, 117861 (2022).
42. Yang, W. T. & Parr, R. G. Hardness, softness, and the fukui function in the electronic theory of metals and catalysis. *Proc. Natl. Acad. Sci. USA* **82**, 6723–6726 (1985).
43. Wang, A. et al. Enhanced and synergistic catalytic activation by photoexcitation driven S–scheme heterojunction hydrogel interface electric field. *Nat. Commun.* **14**, 6733 (2023).
44. Cai, J. et al. Dynamic self-assembly induced rapid dissolution of cellulose at low temperatures. *Macromolecules* **41**, 9345–9351 (2008).
45. Bradford, M. M. Rapid and sensitive method for quantitation of microgram quantities of protein utilizing principle of protein-dye binding. *Anal. Biochem.* **72**, 248–254 (1976).
46. Wolfenden, B. S. & Willson, R. L. Radical-cations as reference chromogens in kinetic studies of one-electron transfer reactions: Pulse radiolysis studies of 2,2′-azinobis-(3-ethylbenzthiazoline-6-sulphonate). *J. Chem. Soc. Perkin Trans.* **2**, 805–812 (1982).
47. Abraham, M. J. et al. Gromacs: High performance molecular simulations through multi-level parallelism from laptops to supercomputers. *SoftwareX* **1-2**, 19–25 (2015).
48. Frisch, M. J. et al. Gaussian 16., Revision C.01 (Gaussian, Inc., 2019).

Acknowledgements

This study was supported by National Natural Science Foundation of China (41821005, X.W. and 41991312, X.W.).

Author contributions

J.Z. and X.W. conceptualized the study and wrote the original draft manuscript. J.Z., J.H., X.Y., C.Y., and L.D. conducted the experiments and analyzed the data. J.C.W., G.V.L., and S.T. contributed review comments and edits to finalize the paper. All authors discussed the results and contributed to the writing of the subsequent versions of the manuscript.

Competing interests

The authors declare no competing interests.

Additional information

Supplementary information The online version contains supplementary material available at https://doi.org/10.1038/s41467-025-58338-9.

Correspondence and requests for materials should be addressed to Xilong Wang.

Peer review information *Nature Communications* thanks the anonymous reviewers for their contribution to the peer review of this work. A peer review file is available.